processes

MDPI

Article

The Investigation of Overflow Water-Powered Projectile-Assisted Injection Molded Short-Glass-Fiber-Reinforced Polypropylene

Wei Zhang, Mao-Zeng Wang, Tang-Qing Kuang *, Qian-Sheng Liao, Shi-Yu Jiang and He-Sheng Liu *

Postdoctoral Station of Transportation Engineering, State Key Laboratory of Performance Monitoring and Protecting of Rail Transit Infrastructure, East China Jiao Tong University, Nanchang 330013, China; weizhang@email.ncu.edu.cn (W.Z.); 15738554319@163.com (M.-Z.W.); liaoqiansheng@163.com (Q.-S.L.); shiyu_jiang@126.com (S.-Y.J.)

* Correspondence: tkuang@ecjtu.edu.cn (T.-Q.K.); hsliu@ecjtu.edu.cn (H.-S.L.)

Abstract: Water-powered projectile-assisted injection molding (W-PAIM) is a novel injection molding technology that has been recently developed based on the ripe water-assisted injection molding (WAIM). Fiber orientation pattern and residual wall thickness (RWT) are two crucial factors determining the quality of W-PAIM parts composed of short fiber-reinforced thermoplastics (SFRTCs). However, limited work has been conducted on W-PAIM of SFRTC parts, which restricts its application process. In this work, an intensive investigation of W-PAIM parts composed of short fiber-reinforced polypropylene was conducted via a newly lab-developed W-PAIM platform. The results indicated that fibers were quite well oriented in the region extending from the core zone to the water channel, especially in the water channel zone, but randomly aligned in a small region near the mold wall. Nevertheless, fibers in the water channel zone of W-PAIM part were highly oriented, presenting an opposite alignment trend in fiber orientation compared to that in the water channel zone of the WAIM part as reported earlier. These disparities in fiber orientation between W-PAIM and WAIM parts were primarily attributed to the strong flow fields generated by projectile penetration. Additionally, the influence of three main processing parameters that significantly affected the projectile penetration on these two crucial factors was also investigated using the single-factor method. It was discovered that water injection delay time constituted the primary factor affecting the projectile penetration process, and reducing this time could greatly increase the relative thickness of the ordered area and the uniformity of RWT. More importantly, within the value range of the tested processing parameters, increased water pressure, elevated melt temperatures, and shorter water injection delay time could simultaneously improve fiber orientation and the uniformity of RWT in W-PAIM parts, which may improve the properties of W-PAIM parts and enlarge their application scope. This work provides a comprehensive guide for the fabrication of W-PAIM parts of SFRTCs.

Keywords: water-powered projectile-assisted injection molding; polymer composites; fiber orientation; residual wall thickness

check for updates

Citation: Zhang, W.; Wang, M.-Z.; Kuang, T.-Q.; Liao, Q.-S.; Jiang, S.-Y.; Liu, H.-S. The Investigation of Overflow Water-Powered Projectile-Assisted Injection Molded Short-Glass-Fiber-Reinforced Polypropylene. *Processes* **2024**, *12*, 2333. https://doi.org/10.3390/pr12112333

Academic Editor: Masoud Soroush

Received: 27 September 2024
Revised: 19 October 2024
Accepted: 22 October 2024
Published: 24 October 2024

Copyright: © 2024 by the authors. Licensee MDPI, Basel, Switzerland. This article is an open access article distributed under the terms and conditions of the Creative Commons Attribution (CC BY) license (https://creativecommons.org/licenses/by/4.0/).

1. Introduction

Water-powered projectile-assisted injection molding (W-PAIM), a novel injection molding technology, has recently developed based on the ripe water-assisted injection molding (WAIM) technology for fabricating hollowed parts [1,2]. The W-PAIM process is presented with a schematic diagram in Figure 1a, and its detailed description is as follows. Initially, a solid projectile is positioned on the water injection inlet; subsequently, the melt is injected into the mold cavity and completely fills the cavity, which is called melt filling process; thirdly, pressurized water drives the projectile to thrust the core of melt ahead into the overflow cavity for the formation of a hollow product; finally, pressurized water continuously proceeds to compact and cool the melt until the melt is thoroughly solidified. The primary difference between W-PAIM and WAIM processes is the utilization of different media to

penetrate the melt, which are a projectile in the W-PAIM process and water in the WAIM process, respectively. Compared with the WAIM process, the W-PAIM process has many advantages due to the involvement of the solid projectile, such as a significant reduction in part weight, shorter cycle time, excellent dimensional stability, less processing cost, wider scope of material applicability, etc. [3–6]. Above all, some crucial indictors determining the application properties of the final molded part, such as the uniformity of residual wall thickness (RWT) and the smoothness of the inner surface, could be significantly improved when using the W-PAIM process, and thus the life span and application range of the final molded part could be remarkably improved [4–6].

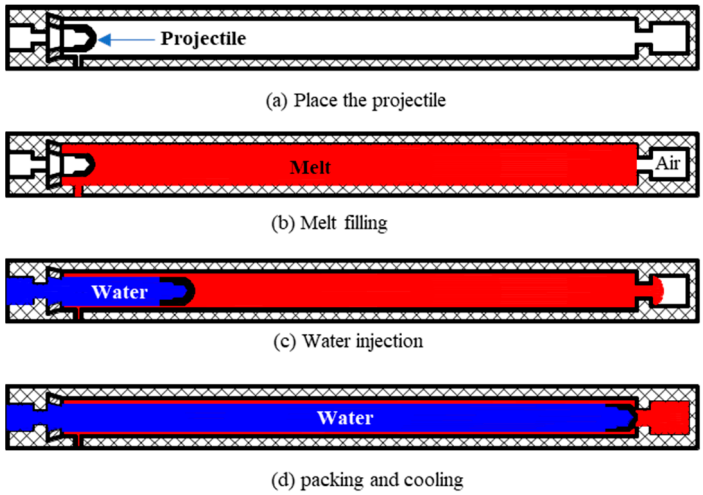

Figure 1. Schematic diagram of W-PAIM process.

Because of its unique advantages, W-PAIM has received extensive attention, and numerous intensive investigations on it have been performed. Current investigations, nevertheless, are mainly concentrated on the influence of numerical simulation models [2], projectile diameter [3], process parameters [3,6], and mold design [6] on the projectile penetration behavior and the RWT of unfilled W-PAIM moldings. The research on W-PAIM parts of short glass fiber-reinforced thermoplastics (SFRTCs) is scarcely reported.

At present, short fibers has been widely employed to enhance the mechanical strength of the products to fulfill the high-performance demands of molded components, and injection-molded SFRTC hollow parts are increasingly replacing metal parts in the fabrication of some structural elements of automobiles under the trend toward lightweight transportation equipment [7–9]. As the RWT and fiber orientation are two crucial factors determining the quality of injection-molded hollow parts of SFRTCs, over the years, significant efforts have been undertaken to study the RWT and fiber orientation employing WAIM. The results showed that the fiber orientation and RWT were determined by water penetration, and more stable water penetration facilitated a more uniform RWT [9–11], while the fiber orientation was influenced by the flow field generated by water penetration and the water penetration behavior within the mold cavity [12–14]. In addition, our previous investigations have demonstrated that compared to the water penetration process in WAIM, the projectile penetration process in W-PAIM is more stable and complex, and the melt is subjected to a larger and more complicated shear action during projectile penetration, suggesting that W-PAIM parts composed of SFRTCs may be processed with a uniform RWT and more ordered fiber orientation [2,6,14]. Therefore, it is vital to study the W-PAIM parts of SFRTCs in more detail, so as to enhance the mechanical performance of the molded parts and facilitate industrial applications of the W-PAIM process.

In this work, W-PAIM parts composed of short-glass-fiber-reinforced polypropylene (SGFRPP) were molded via a newly lab-developed W-PAIM platform in our lab. Then, the evolution mechanism of fiber orientation pattern within the part was clarified with the assistance of a flow field analysis and the projectile penetration behavior. Finally, the effect

of processing parameters on the two main factors affecting the mechanical properties, i.e., RWT and fiber orientation, were investigated by the single-factor method. The findings in this work are expected to provide a comprehensive guide for the fabrication of W-PAIM parts of SFRTCs.

2. Experimental Part

2.1. Materials

For sample molding, 20 wt% SGFRPP (SB224-2, LyondellBasell Industries Co., Ltd., Shanghai, China) was utilized, and its further details can be obtained from our prior investigation [13]. Additionally, polyamide 6 (1010C2, DSM Engineering Plastics, Inc., Tokyo, Japan) was employed in the fabrication of the projectile, of which more detailed information can be obtained elsewhere [6].

2.2. Sample Preparation

The main body of the W-PAIM part of 20 wt% SGFRPP is a straight duct, and its dimensions are 245 mm in length and 16 mm in diameter, as illustrated in Figure 2. All the parts were molded utilizing a lab-developed W-PAIM platform, the specific information of which can be obtained in our earlier research [6]. The projectile used in this work was designed by ourselves; its structure and dimensions are presented in Figure 3.

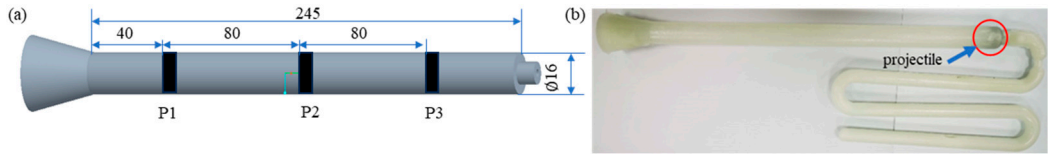

Figure 2. (**a**) Structure and dimensions of the plastic tube, (**b**) sample of plastic tube. (unit: mm).

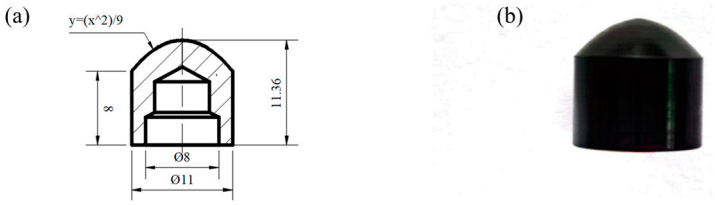

Figure 3. (**a**) Structure and dimensions of the projectile, (**b**) projectile. (unit: mm).

It has been established that the two crucial factors (RWT and fiber orientation) determining the quality of injection-molded hollow parts of SGFRPP are mainly dependent on the fluid penetration within the mold cavity [11,13,14]. In addition, many researchers have demonstrated that the primary processing parameters that significantly affected the projectile penetration of W-PAIM were water pressure, melt temperature, and water injection delay times [5,6]. In this work, therefore, we identified the above three process parameters as the main factors and studied their influence on the two key indicators that determine the quality of W-PAIM parts using a single factor method. Before conducting experimental investigations, preliminary trials were conducted using the processing parameters recommended by the material manufacturer to establish the appropriate ranges for the primary processing parameters. The final values of the primary processing parameters were used in the experiments presented in Table 1; other processing parameters included a melt injection pressure of 80 MPa, along with mold and water temperatures set at 39 °C.

Table 1. The values of processing parameters used in experiments.

Processing Parameters	Values		
Water pressure (MPa)	4	**6**	8
Water injection delay time (s)	1	**3**	5
Melt temperature (°C)	210	**230**	250

Note: The basic values in the table are shown in bold.

2.3. Characterization

As the projectile penetrates the polymer melt along the direction of least resistance under the propulsion of water, the unstable water flow behavior may lead to variations in the RWT and fiber orientation at different positions along the melt flow direction [2,5,12]. To thoroughly understand the influence of the three selected factors on the two indicators that determine the quality of W-PAIM parts, samples with a length of 20 mm were obtained by cutting along the thickness direction for RWT measurement. Moreover, to assess the uniformity of RWT, a variation factor (*VF*) was adopted [7], and its description is as below:

$$FV = \frac{\sigma}{\overline{R}} \quad (1)$$

where σ represents the standard deviation, $\overline{R}$ represents the average value of RWT. Note that the smaller the *FV*, the more uniform the RWT of the molded part. Additionally, it was essential to exclude the RWT measurements at the end of the cavity from the FV calculation, as the variable cross-section in this area led to a considerable fluctuation in the RWT [7].

Furthermore, to thoroughly understand the evolution of fiber orientation within the part molded via W-PAIM, three samples were firstly cut at three different positions of the molded part, as shown in Figure 1. Secondly, the samples were subjected to brittle fracture in liquid nitrogen to obtain fracture surfaces (shown in Figure 4). Finally, these surfaces were coated with gold to enhance conductivity and subsequently observed using a SEM system.

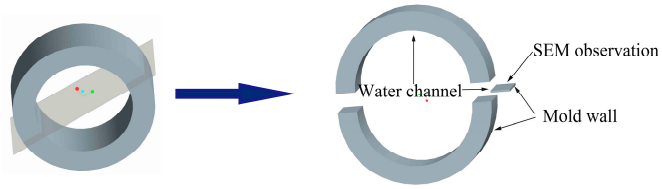

Figure 4. Diagram of sample preparation process for SEM testing.

3. Results and Discussion

3.1. Typical Fiber Orientation Patterns Within W-PAIM Part

The SEM pictures of fiber orientation within the W-PAIM part are shown in Figure 5. Clearly, the fiber orientation across the thickness of the W-PAIM part varied greatly, and the RWT could be divided into three distinct zones based on the fiber orientation pattern, i.e., shell zone, core zone, and water channel zone. Through closer examination, fibers tended to exhibit a random orientation in the shell zone, and many holes were left in this layer because the randomly ranked fibers were broken during the sample preparation process. In contrast, nearly all fibers were quite orderly aligned in the water channel zone, especially those fibers near the water channel. The core zone served as a transition between these two zones, where most fibers aligned along the melt flow direction, except for some near the shell layer that retained random orientations. In summary, the fiber orientation along the flow direction became increasingly ordered as the distance between the position of the fiber and the mold wall increased.

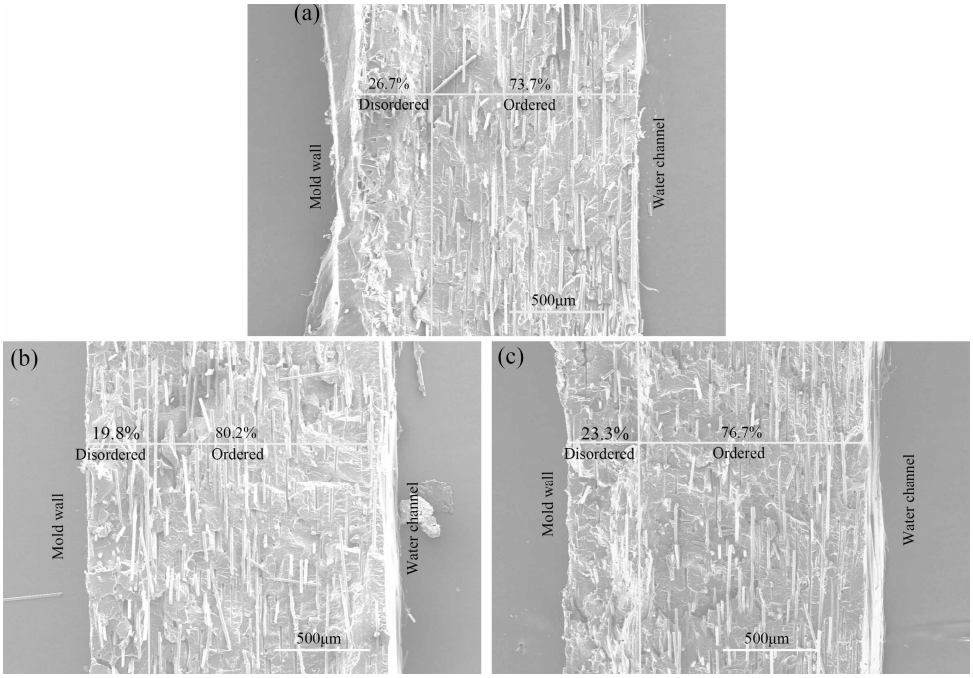

Figure 5. Typical SEM micrographs of the three selected positions: (**a**) P1, (**b**) P2, and (**c**) P3. Water pressure, 6 MPa; melt temperature, 230 °C; water injection delay time, 3 s.

Based on the above observations, it was found that the fiber orientation pattern across the RWT of the W-PAIM parts significantly differed from that in the WAIM parts, particularly in the water channel zone. For a WAIM part, most fibers were quite well-aligned in the core area and randomly aligned in the other two areas [10–12], while in a W-PAIM part, as illustrated in Figure 5, fibers were quite well-oriented in the region extending from the core zone to the water channel, especially in the water channel zone. This notable distinction in fiber orientation between W-PAIM and WAIM parts should be primarily attributed to the strong flow field induced by the projectile penetration in W-PAIM [2,12,15]. It should be noted that facilitating more fiber orientations across the thickness of a part is of crucial for enhancing the mechanical strength of molded fiber-reinforced polymer composites; thus, it is essential to further investigate the evolution mechanism of fiber orientation within the parts molded via W-PAIM [7,12,13].

W-PAIM comprises a dual filling process, namely melt injection and projectile penetration. As illustrated in Figure 1, the melt filling process of W-PAIM closely resembles that of WAIM. In this case, a weak shear stress is generated during the melt filling process of W-PAIM [7,12,14]. Additionally, the melt will be solidified quickly upon contact with the mold wall, and thus, the fiber orientation is also preserved at same time. In addition, the solidified layer will continue to thicken towards the middle of the cavity during the three-second water injection delay period [9,12,16]. As a result, fibers in the area from the mold wall to the core zone near it tended to be randomly aligned along the flow direction.

For the projectile penetration process a solid projectile like a piston moves under the propulsion of pressurized water. A piston flow and a uniform speed region that was similar to the sectional dimension of the projectile itself appeared at the projectile front, which resembled the water penetration process in WAIM [2,5,6]. Thus, at the front of the projectile, the minimum and maximum velocity respectively appeared at the core layer near the mold wall and equal velocity region, while the shear stress demonstrated an inverse trend [2,12,17], that is, a minimum and maximum shear stress respectively appeared at the projectile front and core region near the mold wall, which was in agreement with the previous investigation [2]. In addition, we adopted the Fluent software 14.0 to calculate the penetration process of the projectile in W-PAIM. The same processing conditions as those applied during the experiment were used in the simulation; other

detailed information about the simulation is available elsewhere [6]. The numerical results for velocity distribution at positions P2 are as shown in Figure 6. It was also found that there was a piston flow and a uniform speed region at the leading edge of the projectile. As a result, fibers in the core zone near the water channel zone tended to be ranked orderly.

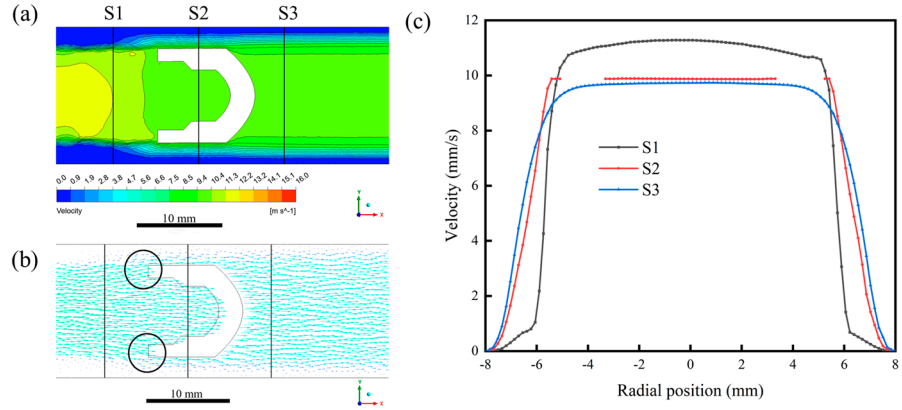

Figure 6. Numerical results for velocity at position P2 of W-PAIM part: (**a**) velocity distribution, (**b**) velocity vector, (**c**) velocity profiles at the positions near the projectile.

Furthermore, according to previous studies, drag flow developed on the both sides of the projectile, leading the RWT of W-PAIM samples to be smaller than the basic one [2,5,6]. As illustrated in Figure 7, the RWT of the molded part in this work was much smaller than the basic one (2.5 mm), and the surface of the projectile had adhered to a thin layer of SGFRPP post-use. These findings suggested that a drag flow also developed on both sides of the projectile in this work, and a great drag force was generated by the projectile penetration, which induced more orderly fiber orientation in the region near the water channel [2,5,6]. Additionally, it can be observed from Figure 6 that the velocity gradient generated by the drag flow was much larger than that generated by the plunger flow. Moreover, the influence of drag flow on the melt velocity gradient became more inconspicuous at melt positions far away from the mold wall, which is in good agreement with the findings reported earlier [2,5,6]. That is, the largest shear stress in W-PAIM appeared at the water channel zone. Therefore, most fibers in the water channel zone of W-PAIM parts were well-ordered, and the notable fiber orientation existed at the region near the water channel. However, numerous researchers have demonstrated that fibers in the area near the water channel of WAIM part experienced a weak shear stress, causing more fibers to be randomly oriented there [12–14].

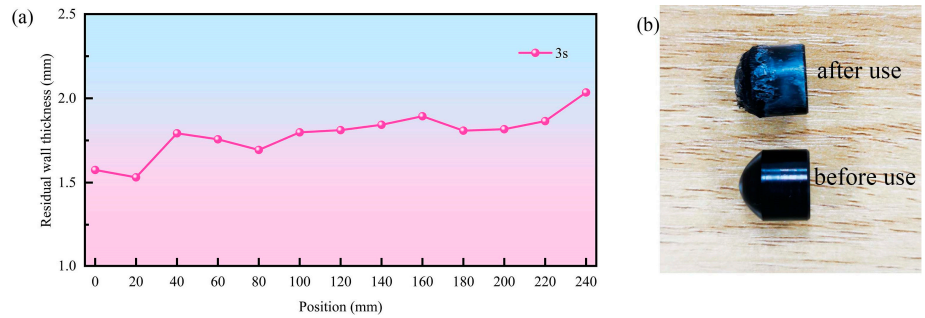

Figure 7. RWT distribution (**a**) and projectile (**b**).

As shown in Figure 3, it can also be clearly seen that the thickness of the ordered regions of fiber orientation at the three selected locations was different. Since differences in the thickness of the sample used for SEM characterization existed, the fiber orientation states at three selected locations were quantitatively characterized by utilizing the relative thicknesses of the ordered/disordered zones, as displayed in Figure 5 [12,13,18]. In the

ordered region, the majority of fibers exhibited ordered alignments along the flow direction, while in the disordered region, their alignments appeared random. As illustrated in Figure 3, the relative thickness of the fiber-ordered region at position P2 was notably greater at 80.2%, in contrast to position P1, which demonstrated the smallest relative thickness of 26.7%.

The following explanation provided clarity on this matter. At the commencement of water injection, the actual pressure value of water was lower than the preset one, resulting in an instability in the penetration behavior of the projectile near the water inlet [2,19,20]. Therefore, at position P1, it was difficult for the projectile to push the melt forward, especially the high-viscosity melt frozen by the mold wall before the projectile arrived there, resulting in a larger disordered region in the core zone near the mold wall and a nonuniformity of RWT distribution, whereas at the end of the part, the end of the cavity was a variable cross-section (shown in Figure 2b), where the melt accumulated [12,21]. With the increase in water injection time, the melt accumulation phenomenon there became more serious, which in turn increased the resistance to projectile penetration. This in turn reduced the strength of the shear stress acting on the fibers, resulting in more random fiber orientation at position P3 [2,6,12]. Figure 7 demonstrates that the RWT changed little between 40 mm and 200 mm from the water injection port, while it exhibited significant variability at both ends of the part. These observations suggested that the water pressure reached the preset level before the projectile arrived at position P2, with instability at the start of the part being more pronounced than at the end [2,12]. Additionally, many investigations had demonstrated that instability of penetration behavior near the water inlet was much more serious than that at other positions, resulting in a larger fiber-disordered region than at other positions [2,13,14]. Consequently, the relative thickness of the fiber-ordered region at position P2 was the largest, and the relative thickness of the ordered region at position P1 was the smallest. These findings also indicated the importance of projectile penetration behavior in the development of fiber orientation. To acquire an excellent-quality W-PAIM part, we further studied the influence of three key processing parameters affecting the projectile penetration on the RWT and fiber orientation within the W-PAIM part.

3.2. Effect of the Processing Parameters on the RWT and Fiber Orientation

3.2.1. Water Pressure

Figure 8 displays the impact of water pressure on the RWT and FV. As can be seen, when the water pressure was maintained at lower levels (ranging from 4 MPa to 6 MPa), increasing it helped the overall RWT of the product become thinner, but it had little difference in improving the wall thickness uniformity. When the water pressure was further raised to a high value (8 MPa), the RWT and FV were reduced, namely, the molded product become thinner and uniform. This phenomenon can be elucidated as follows: raising the water pressure helped the projectile to drag more melt near it forward, resulting in a smaller RWT. Additionally, researchers had demonstrated that when the water pressure was set at a lower value, either lowering it further or raising it to a high value could both improve the instability of the flow behavior of pressurized water at the front of the part [16,22]. Furthermore, higher water pressure was helpful to weaken the influence of melt accumulation at the end of the cavity on the flow behavior of pressurized water there [12]. Consequently, an increase in water pressure from 4 MPa to 6 MPa resulted in a smaller RWT and wall thickness uniformity; while with the water pressure further increased to a high value of 8 MPa, the RWT became smaller and more uniform.

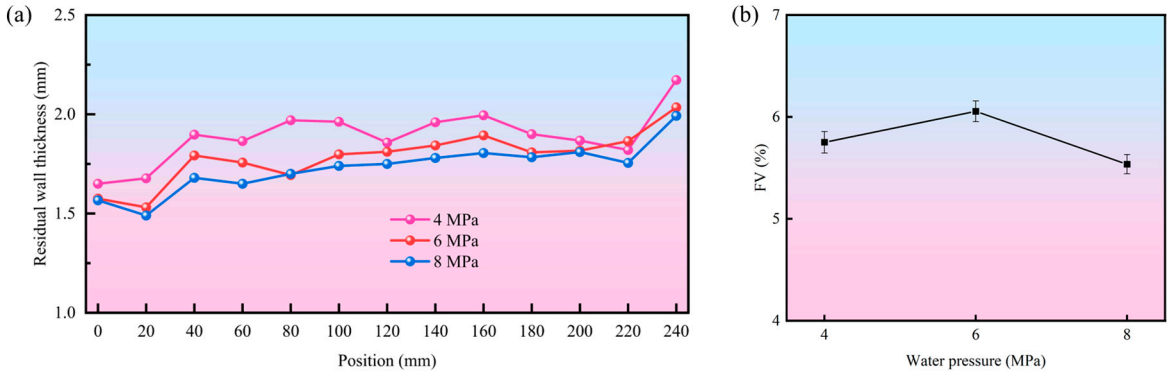

Figure 8. Influence of water pressure on (**a**) RWT, (**b**) FV.

Figures 5 and 9 display the impact of water pressure on the fiber orientation at the designated positions. As shown in Figures 3 and 9, water pressure significantly influenced the fiber orientation. Notably, an increase in water pressure from 4 MPa to 6 MPa resulted in a minor enhancement in the relative thickness of ordered fiber regions. With the water pressure further elevated to 8 MPa, the relative thickness of ordered regions markedly increased. These findings can be attributed as follows. The higher water pressure caused the projectile to push the melt forward faster, leading to a larger velocity gradient across the RWT [12–14]. Namely, shear stress markedly increased. Additionally, both higher water pressure (8 MPa) and lower water pressure (4 MPa) could improve the instability of projectile penetration behavior at position P1 (shown in Figure 8), and this in turn induced more fiber orientation there. Therefore, raising the water pressure from 4 MPa to 6 MPa yielded little difference in fiber orientation, but further increasing the water pressure markedly increased the relative thickness of the ordered regions.

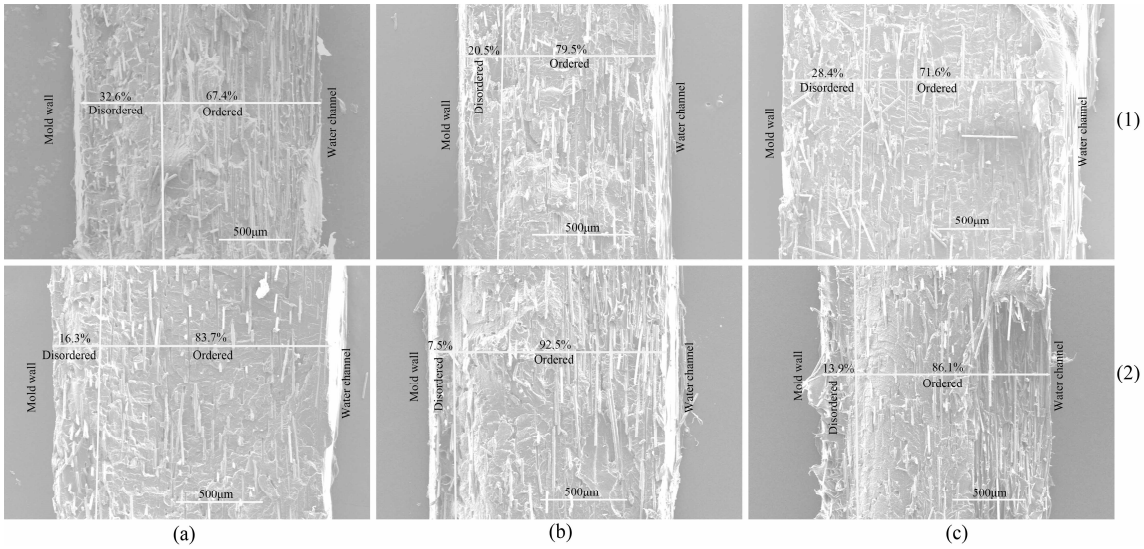

Figure 9. SEM images of the positions (**a**) P1, (**b**) P2, (**c**) P3 within W-PAIM parts molded under the water pressure of (**1**) 4 MPa, (**2**) 8 MPa.

3.2.2. Melt Temperature

Figure 10 displays the effect of melt temperature on the RWT and FV. It was observed that elevating the melt temperature distinctly reduced both the RWT and FV. These findings could be attributed to the following factors. As previously noted, the melt solidified upon contact with the mold wall during the filling process, and this solidified layer continued to thicken toward the middle of the cavity during the delay time. This in turn made it difficult for the projectile to drag the melt around it forward [16,19]. Conversely, upon increasing

melt temperature, the melt viscosity decreased, reducing the resistance to projectile penetration and resulting in a more stable projectile penetration process, which in turn improved the RWT uniformity. On the other hand, the thickness of the solidified layer decreased with increasing melt temperature, resulting in more melt around the projectile being dragged forward, with the RWT thus becoming thinner.

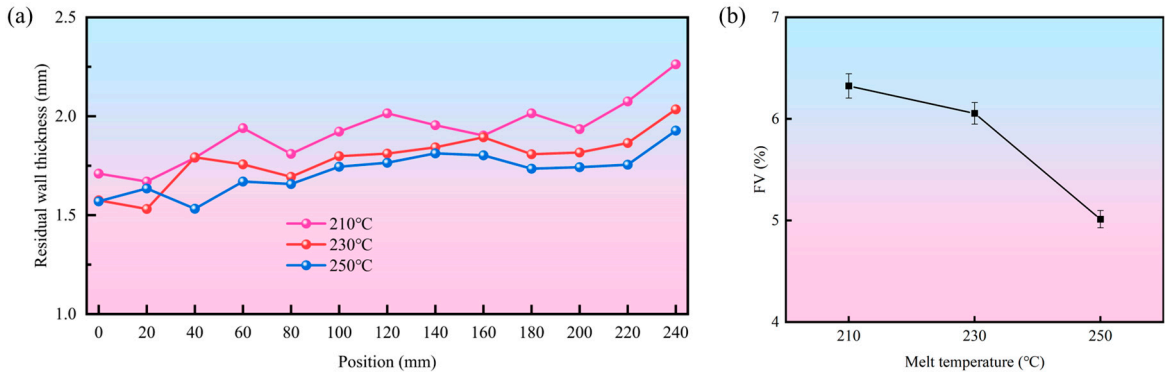

Figure 10. Influence of melt temperature on (**a**) RWT, (**b**) FV.

Figures 5 and 11 display the impact of melt temperature on the fiber orientation at the designated positions. As depicted in Figures 5 and 11, melt temperature markedly affected the fiber orientation, especially the fiber orientation at position P2. When the melt temperature increased to 250 °C, almost all fibers across the RWT at position P2 were aligned orderly. This phenomenon can be attributed to the reduction in melt viscosity that occurred with increasing temperature, resulting in the projectile penetration resistance being markedly decreased, which allowed the projectile to push the melt forward more quickly. This in turn increased the melt velocity gradient across the RWT, and thus the shear stress exerted on the fibers increased. Nevertheless, it is important to note that the impact of higher temperature on the instability of projectile penetration behavior at both ends of the cavity, as depicted in Figure 10, remained minimal. As a result, the increase in melt temperature primarily contributed to more fiber orientation at position P2, with limited effects on fiber orientation at positions P1 and P3.

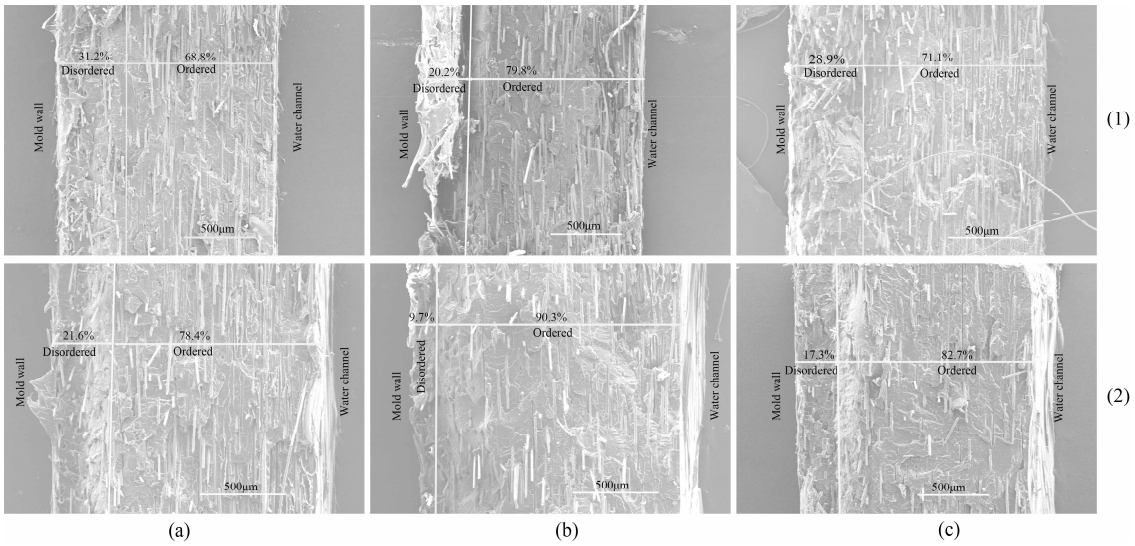

Figure 11. SEM images of positions (**a**) P1, (**b**) P2, (**c**) P3 within W-PAIM parts molded under the melt temperature of (**1**) 210 °C, (**2**) 250 °C.

3.2.3. Water Injection Delay Time

Figure 12 displays the effect of water injection delay time on the RWT and FV. As depicted in Figure 12, an increase in water injection time resulted in the RWT becoming thicker and uneven. The reason for the above observations can be articulated as follows. An increase in water injection delay time extended the duration for the cooling of the melt by the mold wall. This resulted in the solidified layer adjacent to the mold wall continuously thickening toward the middle of the cavity during the delay time [5,6,16]. On the one hand, the melt dragged forward by the projectile decreased, leading to a thicker RWT. On the other hand, the resistance to projectile penetration became larger, leading to an unstable projectile penetration behavior, which, in turn, resulted in a more irregular RWT.

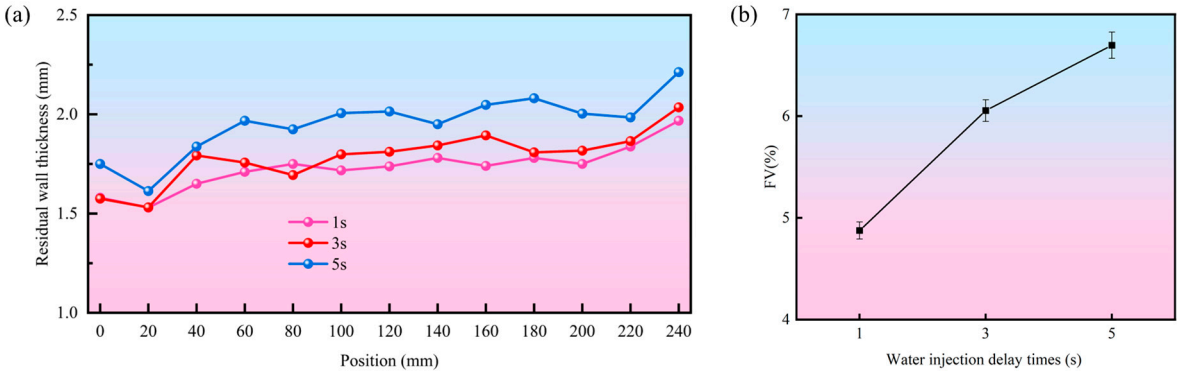

Figure 12. Influence of water injection delay time on (**a**) RWT, (**b**) FV.

Figures 5 and 13 display the impact of water injection delay time on the fiber orientation at the designated positions. As shown in Figures 3 and 11, the duration of delay time significantly affected fiber orientation, particularly at positions P1 and P3. When it was extended to 5 s, most fibers exhibited random orientations in nearly one-third of the thickness of the RWT at these two positions. The reason for the above observations can be articulated as follows. As previously noted, extending the water injection delay time resulted in less melt around the projectile being dragged forward, which, in turn, diminished the area of the melt exposed to an intense shear stress [5,13,14]. Additionally, longer delay time could aggravate the unstable projectile penetration behavior at both ends of cavity (shown in Figure 12) [5,13,16]. As a result, extending the delay time led to more random fiber orientations at the designated positions, particularly at positions P1 and P3.

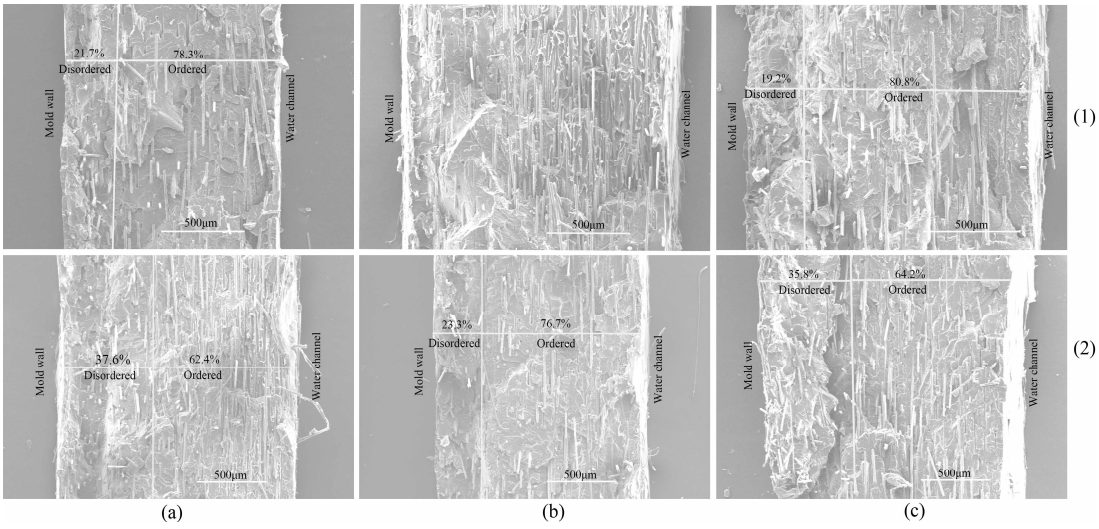

Figure 13. SEM images of the positions (**a**) P1, (**b**) P2, (**c**) P3 in W-PAIM parts molded under the water injection delay time of (**1**) 1 s, (**2**) 5 s.

Furthermore, although raising water pressure and melt temperature could significantly increase the shear stress exerted on the fibers, the fibers in the shell layer still presented random orientations, whereas reducing water injection delay time could significantly facilitate a more orderly alignment of fibers in this area. This finding further proved that the mold wall had an effective cooling impact on the melt, and that water injection time was the main factor affecting the projectile penetration and fiber orientation.

4. Conclusions

In this work, the fiber orientation pattern and RWT within W-PAIM parts were intensively investigated. The findings indicated that the characteristic hierarchical structure of fiber orientation, typically identified in WAIM parts—comprising a 'shell layer-core layer-water channel layer', was also presented in W-PAIM components; however, the fiber orientation distributions at these three specific layers between W-PAIM and WAIM parts presented a great difference due to the strong shear generated by projectile penetration. In a W-PAIM part, fibers located from the core region near the mold wall to the water channel, particularly those adjacent to the water channel, exhibited a highly ordered alignment along the flow direction, while those near the mold wall exhibited random alignment. Additionally, the results also indicated that the processing parameters affecting the projectile penetration had a decisive effect on both fiber orientation pattern and RWT. Within the value range of the tested processing parameters, higher water pressure, elevated melt temperatures, and shorter water injection delay times could simultaneously improve fiber orientation and the uniformity of RWT in W-PAIM parts. This work is expected to provide a guide for the fabrication of W-PAIM parts of SFRTCs. However, our research concentrated only on three main processing factors without considering other factors and the interactions among them, or the influences of different types of polymer resins, leading to the limitations of our research. Further investigations on the interactions among processing factors should be performed. Additionally, other equipment capable of observing fiber orientation states in three-dimensional space, such as computed tomography (CT), should be utilized to better guide the practice of forming W-PAIM parts composed of SFRTCs.

Author Contributions: Writing—original draft, Formal analysis, Writing—review and editing, Project administration, Funding acquisition, Supervision, W.Z.; Investigation, M.-Z.W.; Writing—review and editing, Supervision, Project administration, Funding acquisition, T.-Q.K.; Methodology, Investigation, Q.-S.L.; Methodology, Investigation, S.-Y.J.; Writing—review and editing, Supervision, Project administration, H.-S.L. All authors have read and agreed to the published version of the manuscript.

Funding: This work is financially supported by the National Natural Science Foundation of China (NSFC, Nos, 52303038, 52163006, 52273033), Major Basic Research Projects of Jiangxi Province (No. 20223BBE51012), and Jiangxi Provincial Science and Technology Plan of China (No. GJJ2202407).

Data Availability Statement: Data sharing is not applicable to this article as no new data were created or analyzed in this study.

Acknowledgments: The authors are very grateful for the financially supporting.

Conflicts of Interest: The authors declare no conflicts of interest.

References

1. Kuang, T.Q.; Liu, T.; Feng, Q.; Liu, W.W.; Liu, H.S.; Turng, L.S. Fluid-Powered Projectile-Assisted Injection Molding: Principles and Developments. *Int. Polym. Proc.* **2020**, *35*, 2–15. [CrossRef]
2. Kuang, T.; Feng, Q.; Liu, T.; Zhong, L.; Wang, Y.; Liu, H. Numerical Simulation on the Penetration Behavior of the Projectile during the Water Injection Stage of Water-Projectile-Assisted Injection Molding Process. *Adv. Polym. Tech.* **2020**, *1*, 6861216. [CrossRef]
3. Gründler, M.; Hildebrand, T. Method for Producing Polymeric Hollow Portion, Involves Forming Cavity with Respect to Displacement of Fluent Molding Material. DE Patent 102011100132, 30 April 2011.
4. Eckardt, H. Lightweighting: Making Parts Lightweight & Strong with New Technologies. *Plast. Tech.* **2022**, *57*, 30–32.
5. Ding, J.X.; Chen, Y.L.; Zhou, H. Effect on residual wall thickness of parts with floating core injection of water-assisted injection molding. *J. Zhejiang Univ.-Eng. Sci.* **2017**, *51*, 937–945.

6. Kuang, T.Q.; Pan, J.Y.; Feng, Q.; Liu, H.S.; Xu, B.P.; Liu, W.W.; Turng, L.S. Residual wall thickness of water-powered projectile-assisted injection molding pipes. *Polym. Eng. Sci.* **2019**, *59*, 295–303. [CrossRef]
7. Tseng, H.C.; Chang, R.Y.; Hsu, C.H. Accurate predictions of orientation dependent modulus in short-fiber-reinforced composite with experimental validation. *Polym. Compos.* **2018**, *39*, 2847–2859. [CrossRef]
8. Mortazavian, S.; Fatemi, A. Fatigue behavior and modeling of short fiber reinforced polymer composites including anisotropy and temperature effects. *Int. J. Fatigue* **2015**, *77*, 12–27. [CrossRef]
9. Jiang, Q.; Zhang, W.; Wan, Z.; Zhou, H.; Jiang, S.; Nie, H. Experimental and numerical investigations on formation mechanisms of hollow structures in overflow water-assisted injection-molded parts of short-glass-fiber-reinforced polypropylene. *J. Appl. Polym. Sci.* **2024**, *141*, e55916. [CrossRef]
10. Liu, S.J.; Chen, Y.S. The manufacturing of thermoplastic composite parts by water-assisted injection-molding technology. *Compos. Part A Appl. Sci. Manuf.* **2004**, *35*, 171–180. [CrossRef]
11. Yang, J.; Yu, S. Prediction of process parameters of water-assisted injection molding based on inverse radial basis function neural network. *Polym. Eng. Sci.* **2020**, *60*, 3159–3169. [CrossRef]
12. Zhang, W.; Liu, H.S.; Jiang, Q.S.; Kuang, T.Q.; Lai, J.M.; Huang, X.Y. Formation mechanism of high-pressure water penetration induced fiber orientation in overflow water-assisted injection molded short glass fiber-reinforced polypropylene. *J. Appl. Polym. Sci.* **2021**, *138*, 50960. [CrossRef]
13. Huang, H.X.; Zhou, R.H.; Yang, C. Fiber orientation propelled by high-pressure water penetration in water-assisted injection molded fiber-reinforced thermoplastics part. *J. Compos. Mater.* **2013**, *47*, 183–190. [CrossRef]
14. Zhang, W.; Kuang, T.Q.; Liu, H.S.; Lai, J.M.; Han, J.K.; Jiang, Q.S.; Wan, Z.H. Improved process moldability and part quality of short-glass–fiber-reinforced polypropylene via overflow short-shot water-assisted injection molding. *J. Polym. Eng.* **2022**, *42*, 362–373. [CrossRef]
15. Zheng, G.Q.; Yang, W.; Huang, L.; Yang, M.B.; Li, W.; Liu, C.T.; Shen, C.Y. Flow-induced fiber orientation in gas-assisted injection molded part. *Mater. Lett.* **2007**, *61*, 3436–3439. [CrossRef]
16. Liu, X.-H.; Huang, H.-X. Effects of processing conditions on melt flow of water assisted melt filling. *J. Chem. Eng.* **2011**, *62*, 520–524.
17. Liu, S.J.; Lin, W.R.; Lin, K.Y. Morphological development in water assisted injection molded polyethylene/polyamide-6 blends. *Polym. Adv. Technol.* **2011**, *22*, 2062–2068. [CrossRef]
18. Yang, C.; Huang, H.X.; Li, K. Investigation of fiber orientation states in injection-compression molded short-fiber-reinforced thermoplastics. *Polym. Compos.* **2010**, *31*, 1899–1908. [CrossRef]
19. Yang, J.-G.; Zhou, X.-H.; Niu, Q. Model and simulation of water penetration in water-assisted injection molding. *Int. J. Adv. Manuf. Tech.* **2013**, *67*, 367–375. [CrossRef]
20. Wu, Y.C.; Liu, S. Flow visualisation of water assisted injection moulding process. *Plast. Rubber Compos.* **2005**, *34*, 227–231. [CrossRef]
21. Yang, J.-G.; Zhou, X.-H. Numerical simulation on residual wall thickness of tubes with dimensional transitions and curved sections in water-assisted injection molding. *J. Appl. Polym. Sci.* **2012**, *128*, 1987–1994. [CrossRef]
22. Zhang, Z.M.; Zhou, H.; Gao, Y.N.; Yang, H.Y. Simulation and Analysis on Cavity Filling Process in Water-assisted Injection Molding. *J. Mech. Eng.-Chin.* **2010**, *46*, 140–146. [CrossRef]

Disclaimer/Publisher's Note: The statements, opinions and data contained in all publications are solely those of the individual author(s) and contributor(s) and not of MDPI and/or the editor(s). MDPI and/or the editor(s) disclaim responsibility for any injury to people or property resulting from any ideas, methods, instructions or products referred to in the content.